Influence of Nanoparticle Surface Chemistry on Ion Transport in Polymer Nanocomposite Electrolytes

Santosh Mogurampelly* and Venkat Ganesan*

Department of Chemical Engineering, University of Texas at Austin, Austin, Texas 78712, United States.

E-mail: santoshcup6@gmail.com; venkat@che.utexas.edu

Phone: 512-471-4856

Abstract

Using atomistic molecular dynamics simulations, we study the ion diffusivities and conductivities of polyethylene oxide polymer electrolytes doped with $LiBF_4$ salt and containing dispersed Al_2O_3 nanoparticles. We consider nanoparticles of two different surface chemistries: (a) containing acid rich surface sites (α-Al_2O_3); (b) containing roughly equal acidic and basic surface sites (γ-Al_2O_3). We compare the ionic diffusivities and conductivities of such systems with our earlier results [Mogurampelly et al. *Macromolecules* 2015, **48**, 2773-2786] for systems containing basic surface sites on the nanoparticles (β-Al_2O_3). In the presence of α-Al_2O_3 and γ-Al_2O_3 nanoparticles, we observe a monotonic decrease of ionic conductivities and mobilities with particle loading. These results are consistent with our earlier findings in the context of β-Al_2O_3 nanoparticles. Our analysis identifies that the ionic mobilities and conductivities correlate with the combined effects of the changes in polymer segmental dynamics and the modifications in the local environment of ionic species arising from the introduction of nanoparticles.

1 Introduction

Polymer electrolytes containing nanosized ceramic fillers, also termed as polymer nanocomposites (PNCs), have recently emerged as an active research area in the context of development of advanced rechargeable batteries.[1–12] Experiments have demonstrated for some parametric conditions that adding micron or nano-sized electrochemically inert ceramic filler particles like TiO_2, SiO_2, Al_2O_3 to polymer electrolytes, may enhance the conductivity of the underlying matrix.[5–7,13] These results have sparked an intense interest in developing a fundamental understanding of the mechanisms underlying the ion transport properties of polymer nanocomposites.

Inspired by the above results, in a recent study we used all atom molecular dynamics and trajectory-extending kinetic Monte Carlo simulations, to study the influence of β-Al_2O_3 nanoparticles (i. e. Al_2O_3 nanoparticles containing basic surface sites) on the transport properties of polyethylene oxide (PEO) melt solvated with $LiBF_4$ salt.[14] We observed that the mobility of Li^+ cations, BF_4^- anions and the overall conductivity decreased upon the addition of nanoparticles. Our analysis indicated that the nanoparticles slow the dynamics of polymer segments near their surfaces. Moreover, the preferential interactions of the ions with the nanoparticles was seen to lead to an enhancement of ion concentration near the particle surfaces. Together, these effects were seen to increase the residence times of Li^+ cations near the polymer backbone in the vicinity of the nanoparticles and reduce the overall mobility and conductivity of the electrolyte. Similar results have also been reported by others[15,16] for PEO-LiX-Al_2O_3 where X=(Cl^-, Br^-, I^- and BF_4^-) and for PEO containing dispersed TiO_2 nanoparticles.[17–19]

Transport of ions in PNCs is believed to be influenced by a number of different mechanisms which include, ion motion mediated by polymer segments, nanoparticle-ion and nanoparticle-polymer interactions, modulation of the polymer conformations and amorphicities induced by the addition of nanoparticles etc.[14,17–23] Among the different controlling factors, the nanoparticle-polymer and nanoparticle-ion interactions have been speculated to be important factors in influencing the extent of increase or decrease of ion conductivities in PNCs. For instance, Wiec-

zorek et al.[24] studied the effect of alumina halides and α-Al_2O_3 nanoparticles (i. e. Al_2O_3 nanoparticles containing acidic surface sites) on the properties of polymer electrolytes and correlated their conductivity observations to the strength of Lewis acid-base interactions of the nanoparticles with the ions. In a recent study, Ganapatibhotla and Maranas[22] studied the effect of the surface chemistry of the nanoparticles and found that the presence of acidic surface sites on the nanoparticles could lead to an increase in the conductivity of the electrolyte when compared with nanoparticles containing (roughly) equal numbers of acidic and basic surface sites.

Motivated by the above findings, in this work we seek to extend our earlier results[14] to explicitly study the influence of the surface chemistry on the transport of ions in polymer electrolytes containing Al_2O_3 nanoparticles. Towards this objective, we explicitly model α and γ-Al_2O_3 nanoparticles dispersed in PEO electrolyte using fully atomistic MD simulations and study the ion mobilities and overall conductivity. We model α-Al_2O_3 nanoparticles as containing a large number of acidic sites on the surface, and the γ-Al_2O_3 nanoparticles as containing comparable number of acidic and basic surface sites. We compare the results for such cases with those presented in our earlier article for PEO electrolytes dispersed with β-Al_2O_3 nanoparticles.[14] In such a context, we showed that the magnitudes of reduction in the ionic mobilities and conductivities were *quantitatively* correlated to the changes in the polymer segmental dynamics arising from the introduction of nanoparticles. In the present work, we investigate the universality of such observations for different surface chemistries on the nanoparticles. Within such a context, we also examine other possible mechanisms for the influence of the nanoparticles (specifically, the surface chemistry) upon ion transport characteristics.

We note that there have been some recent work related to the issues discussed in this article. Wick[25] group reported results of computer simulations study of the influence of acidic sites on Al_2O_3 *surfaces* upon ion mobilities in PEO-$LiClO_4$ polymer electrolytes. They employed a united atom model for PEO chains and atomistic model for both the Al_2O_3 *surface* and $LiClO_4$ salt. Using parameterized Lennard-Jones interactions resulting from the fitting of the binding energy obtained from quantum chemical calculations, they observed slightly enhanced ion mobilities

at 323 K, but found no significant changes to the conductivity. Further, they also found increased binding of Li^+ ions to the EO of the polymer chains which leads to increased residence times of Li^+ ions near polymer backbone. In a related work, Eilmes and Kubisiak[26] employed polarizable force fields and also observed similar results in PEO-$LiClO_4$ polymer electrolytes but with acidic Al centers as additives. Moreover, Eilmes and Kubisiak[26] found increased free ions and transference numbers, but reduced conductivity when acidic Al centers were present in the electrolyte.

While the above studies have furnished important insights into the influence of acidic sites on ion transport, to our knowledge, there have been no similar studies in the context of polymers containing dispersed nanoparticles. Some issues specific to nanoparticles include the role of nanoparticle loading, curvature of the nanoparticles etc. Moreover, in our work we seek to compare three different surface chemistries for the nanoparticles while keeping all other parameters the same. Such a study is expected to shed insights on the specific role of surface chemistry of the nanoparticles.

The organization of the rest of the article is as follows: In section 2, we describe the details of the force fields used in our MD simulations. This is followed by a description of the molecular modeling and simulation methods used to study the transport properties of the PEO-$LiBF_4$ electrolyte. In section 3, we present results for the ionic diffusivities and conductivities in the presence of α and γ-Al_2O_3 nanoparticles and compare with those in the presence of β-Al_2O_3 nanoparticles. In section 4, we identify the mechanisms underlying transport properties of polymer nanocomposites presented in section 3. Specifically, we present results of polymer segmental dynamics (section 4.1) and examine the correlations between such results and the diffusivities of the of ions (section 4.2). In section 4.3, we discuss the influence of acidity on the coordination between different components of the polymer nanocomposite. In section 5, we present a summary of our findings.

2 Simulation Details and Quantification Measures

2.1 Force Fields for PEO-$LiBF_4$ Electrolyte

A number of earlier studies have used molecular dynamics simulations with atomistic models of PEO both in the presence and absence of ions, to elucidate the structural and dynamical properties of electrolyte systems.[27–29] For instance, Smith et al.[27] explored the conformational properties of large molecular weight PEO chains and obtained good agreement with the findings of small angle neutron scattering experiments. In other contexts, Müller-Plathe[28] and Neyertz et al.[29] have respectively studied the transport properties of Li^+ and Na^+ ions in PEO matrices. In a series of seminal articles, Borodin and Smith[17,18,30–32] presented many-body polarizable force fields for PEO-Li melt system with various anions. With the use of such force fields, they studied various ion transport properties at the atomistic level and provided fundamental insights into the underlying mechanisms. However, due to the requirement of the long computational times for equilibration of ionic species in the polymer environment, and the many-body nature of the polarizable force fields, Borodin and Smith[17,18,31,32] re-parameterized such interactions to fit to an approximate pair-wise additive form. The parameters in such a force field were systematically fit to preserve various static, dynamic and thermodynamic properties of PEO-salt systems.[17,18,31,32]

Inspired by the success of the two-body interaction approximation parameterized by Borodin and Smith,[17,18,31,32] in the present work, we used the following interaction potential to describe PEO-$LiBF_4$-nanoparticles system:

$$U(\boldsymbol{r}) = U^{\text{bonded}}(\boldsymbol{r}) + Ae^{-Br} - \frac{C}{r^6} + \frac{q_1 q_2}{4\pi\epsilon_0 r} - \frac{D}{r^4}, \tag{1}$$

where bonded interactions, $U^{\text{bonded}}(\boldsymbol{r})$ has contributions arising from all intramolecular bonds, angles and torsions in the PEO-$LiBF_4$ melt. Non-bonded interactions, $U^{\text{nb}}(r)$ included Buckingham potentials (the 2$^{\text{nd}}$ and 3$^{\text{rd}}$ terms) for the short range interactions, Coulomb potential

for long range electrostatics (4^{th} term) and mean-field like approximated form of the dipole polarization interaction (last term).[17,18,31,32] Bonds in PEO-$LiBF_4$ melt were modeled with a harmonic potential of the form $k_r(r-r_0)^2$, angles with $k_\theta(\theta-\theta_0)^2$ and torsions with $\sum_{n=1}^{4} k_\phi(1-\cos(n\phi))$ potential. The force field parameters for PEO-$LiBF_4$ were borrowed from the works of Borodin and Smith.[31,32]

2.2 Force Fields for Al_2O_3 Interactions with PEO-$LiBF_4$ Electrolyte

In this work, we compare our results for α and γ-Al_2O_3 nanoparticle with results we previously reported for β-Al_2O_3 nanoparticles.[14] For the interaction of β-Al_2O_3 nanoparticles with PEO-$LiBF_4$ electrolyte, we use the force field parameters developed by Thomas research group.[15,16,33] To model the surface chemistry of α-Al_2O_3 and γ-Al_2O_3 nanoparticles, we attach H atoms to O_{Al} of Al_2O_3 nanoparticles. We represented the acidic surface chemistry of α-Al_2O_3 nanoparticles by modeling such systems as Al_2O_3 nanoparticles containing specified number of OH groups on the surface. The γ-Al_2O_3 nanoparticles were modeled as Al_2O_3 nanoparticles containing roughly a equal number of OH sites and O_{Al} sites on the surface. Explicitly, surface functionalization of Al_2O_3 nanoparticles with 24 H atoms was used to create α-Al_2O_3 and a functionalization with 12 H atoms was used to model γ-Al_2O_3 nanoparticles. An additional 12 O and 6 O atoms were respectively attached to the α-Al_2O_3 and γ-Al_2O_3 surfaces to render the nanoparticles charge neutral. Schematic of the models adopted for α, β and γ-Al_2O_3 nanoparticles are displayed in Fig. S1 of the electronic supplemental information (ESI). We assumed identical partial atomic charges and interaction parameters applied for O_{Al} atoms attached with H and those of O_{Al} which did not have H atoms attached. However, it should be noted that the interaction parameters of O_{Al} atoms attached with H atoms could be different from the parameters of O_{Al} not attached to H atoms.[25] However, such a parameterization requires quantum mechanical calculations and we did not undertake such an effort here. The H atoms attached to O_{Al} carry partial atomic charges but the non-bonded parameters are neglected. The static partial atomic charges for atoms in β-Al_2O_3 nanoparticles were obtained from Ref. 34.

2.3 Equilibration and Setup

The setup of the initial conformations, equilibration procedure employed and the details regarding the implementation of trajectory-extending kinetic Monte-Carlo (TEKMC) method are identical to the details provided in our previous work.[14] To maintain brevity, here we only briefly summarize the simulation details: an initially low density configuration of the PEO matrix containing 40 chains with chemical structure of H-[CH_2-O-CH_2]$_{55}$-H was solvated with an appropriate number of Li^+ and BF_4^- ions to obtain the desired salt concentration of EO:Li=15:1 and EO:Li=8:1. The molecular weight of the simulated PEO matrix is 2.425 kg/mol. The PEO-$LiBF_4$ matrix was equilibrated to obtain observed experimental density at 1 atm pressure. The roughly spherical Al_2O_3 nanoparticles of diameter 14 Å were dispersed in the bulk PEO-$LiBF_4$ melt to generate different PNC systems containing 5-20 weight percent (wt %) of nanoparticles. The PEO-$LiBF_4$-Al_2O_3 composites having different salt concentrations and different nanoparticle weight percentages were simulated at different temperatures *viz.,* 500 K, 425 K and 350 K. Simulations were performed using LAMMPS[35] at constant number of particles, pressure and temperature (NPT) ensemble to simulate a trajectory of 20 ns in each case.

The final configuration of PEO-$LiBF_4$ melt dispersed with nanoparticles at 500 K and 20 ns was then annealed to 425 K, and subsequently the configuration at 425 K after evolving for 20 ns was annealed to 350 K. The details of the systems we studied are summarized below:

- Nanoparticle-free PEO-$LiBF_4$ melt at 500 K, 425 K and 350 K at two salt concentrations,
- PEO-$LiBF_4$ melt dispersed with both α-Al_2O_3 and γ-Al_2O_3 nanoparticles:
  - Particle loadings of 5, 10 and 20 wt% with EO:Li=15:1 at 500 K, 425 K and 350 K;
  - Particle loadings of 5, 10 and 20 wt% with EO:Li=8:1 at 500 K, 425 K and 350 K.

All the results presented in this article were obtained from analyzing the last 15 ns of the trajectory in conjunction with the TEKMC method.[14] We performed molecular dynamics simulations by keeping the position of the nanoparticles fixed. This is expected to be a reasonable ap-

proximation since the diffusivity of the nanoparticles is typically much less compared to those of polymers and ions in the system. However, to understand the influence, if any, arising from the distribution of the positions of the nanoparticles, we also studied three different random configurations of nanoparticle positions for all loadings at a temperature of 425 K. Snapshots of different configurations of the α-Al_2O_3 nanoparticles at 10 and 20 wt% are shown in Figs. S2 and S3 of ESI, respectively. The ion diffusivity results for the different configurations (Fig. S4 of ESI) were found to be comparable within error bars.

2.4 Quantification Measures

We used a variety of static and dynamical measures to characterize our results and the underlying mechanisms. The static measures were primarily based on the radial distribution functions $g(r)$ and the coordination numbers (CN) identifying the distribution of different atoms in the vicinity of each other and the nanoparticles. For the latter, the local environment of each species was used to calculate the number of atoms of type X around a given atom within a spherical volume of radius, r:

$$\mathrm{CN}_X(r) = 4\pi\rho \int_0^r r'^2 g(r')\mathrm{d}r' \tag{2}$$

where ρ denotes the density of atoms of type X and $g(r)$ represents the radial distribution function between the atoms of interest. In most cases, we calculated CN within the first coordination shell of a given atomic pair and denote the results as CN$\equiv$ CN$_X(r_c)$, where r_c is the chosen cutoff based on the radial distribution function.

Most of the dynamical measures used in the present work were also employed in our previous article,[14] and hence we only provide a brief recap of the terminologies below.

Mean-squared Displacements and Diffusivity: The transport properties of both the cations and anions were probed by calculating the mean squared displacement MSD = $\langle\big(\boldsymbol{R}(t) - \boldsymbol{R}(0)\big)^2\rangle$ (where $\boldsymbol{R}(t)$ denotes the position of the ions at the time t, and $\langle\cdots\rangle$ denote an ensemble average)

at various salt concentrations, temperatures and weight percentages of the nanoparticles. The MSDs were then used to calculate the diffusion coefficient (D) of ions using Einstein relation,

$$D = \lim_{t\to\infty} \frac{1}{6t} \langle \big(\boldsymbol{R}(t) - \boldsymbol{R}(0)\big)^2 \rangle . \tag{3}$$

Ionic Conductivity: Ionic conductivity was calculated using the Einstein relation,

$$\sigma = \lim_{t\to\infty} \frac{e^2}{6tVk_BT} \sum_i \sum_j \langle z_i z_j \big(\boldsymbol{R}_i(t) - \boldsymbol{R}_i(0)\big)\big(\boldsymbol{R}_j(t) - \boldsymbol{R}_j(0)\big)\rangle \tag{4}$$

where e is the electronic charge, z_i is charge of ion i, V is the volume of the simulation box, k_B is the Boltzmann's constant, T is the absolute temperature and $\langle \ldots \rangle$ represents ensemble average. The above equation can be decomposed into

$$\sigma = \sigma_{\text{uncorr}} + \sigma_{\text{corr}} \tag{5}$$

where, σ_{uncorr} and σ_{corr} are respectively given by

$$\sigma_{\text{uncorr}} = \lim_{t\to\infty} \frac{e^2}{6tVk_BT} \sum_i \langle z_i^2 \big(\boldsymbol{R}_i(t) - \boldsymbol{R}_i(0)\big)^2 \rangle \text{ and,} \tag{6}$$

$$\sigma_{\text{corr}} = \lim_{t\to\infty} \frac{2e^2}{6tVk_BT} \sum_i \sum_{j>i} \langle z_i z_j \big(\boldsymbol{R}_i(t) - \boldsymbol{R}_i(0)\big)\big(\boldsymbol{R}_j(t) - \boldsymbol{R}_j(0)\big)\rangle. \tag{7}$$

The first term σ_{uncorr} is the sum of mean squared displacement of the individual ions and can be directly computed from the self diffusion coefficient of ionic species. The second term accounts for cross-correlations between the different ions for $i \neq j$. The degree of uncorrelated ion motion is defined as $\alpha(t) = \sigma/\sigma_{\text{uncorr}}$.[36–39] A value of $\alpha = 1$ corresponds to the situation of maximum conductivity, whereas, $\alpha = 0$ corresponds to the case in which cations and anions move together as ion-pairs giving rise to zero overall conductivity.

The details of the computation of σ were presented in our previous article.[14] In brief, we adopt a procedure proposed in References 36–39. Explicitly, we use the long-time statistics and

MSDs to calculate accurate values for the uncorrelated component σ_{uncorr}. However, instead of calculating σ_{corr}, we use the short-time atomistic statistics to calculate the degree of uncorrelated ion motion $\alpha(t)$.[36–39] The time average value of $\alpha(t)$ in the subdiffusive regime, denoted henceforth as $\bar{\alpha}$, was then used to calculate the overall conductivity as: $\sigma = \bar{\alpha}\sigma_{\text{uncorr}}$. The quantity $\bar{\alpha}$ can be construed as a measure of the number of free charge carriers in the system.

Polymer Segmental Dynamics: To probe the segmental dynamics of the PEO chains, we calculated the autocorrelation function of dihedral angle involving C-O-C-C atoms using[18,40–42]

$$C_{\phi\phi}(t) = \frac{\langle \cos\phi(t)\cos\phi(0)\rangle - \langle\cos\phi(0)\rangle^2}{\langle \cos\phi(0)\cos\phi(0)\rangle - \langle\cos\phi(0)\rangle^2}, \tag{8}$$

where $\phi(t)$ is the dihedral angle involving C-O-C-C atoms in PEO chain at time t. The results of $C_{\phi\phi}(t)$ were fitted to a Kohlrausch-Williams-Watts (KWW) stretched exponential function of the form, $\exp(-(t/t^*)^{\beta})$ (where t^* and β are fitting parameters), and the mean segmental relaxation time, τ of the polymer was extracted as

$$\tau = \int_0^{\infty} \exp\left[-\left(\frac{t}{t^*}\right)^{\beta}\right] dt = t^*\Gamma\left(1+\frac{1}{\beta}\right) \tag{9}$$

where Γ denotes the Gamma function.

Interfacial Effects: To quantify the interfacial effects arising from the presence of nanoparticles we divided the simulation cell into regions "near" and "far" from the nanoparticle surfaces based on the partial radial distribution functions of the nanoparticles with polymer chains. Explicitly, a cutoff distance of 8 Å was used and the center of mass of the four atoms (C-O-C-C) involved in a dihedral angle was used to classify the dihedral angles (i. e. polymer segments) as either "near" or "far" from the nanoparticles. Subsequently, the polymer segmental relaxations $C(t)$ (eq 8) were probed individually for the "near" and "far" regions in the simulation.

3 Results

3.1 Ion Diffusivities in PEO-$LiBF_4$ Electrolyte

3.1.1 Diffusivities at EO:Li=15:1

Figure 1 displays the diffusivities for cations and anions at EO:Li=15:1 salt concentration as a function of the loading of the α, β and γ-Al_2O_3 nanoparticles at various temperatures. Results for D_{Li^+} and $D_{BF_4^-}$ in the presence of β-Al_2O_3 nanoparticles were reported in our previous work,[14] but are shown here for comparison. From Fig. 1(a), we observe that the diffusivity of Li^+ ions increases with increasing temperature, a result consistent with the expectations of increased polymer segmental mobilities at higher temperatures. Secondly, we observe that the mobilities of the anions are higher than that of cations, a result also in agreement with our earlier reports.[14,31]

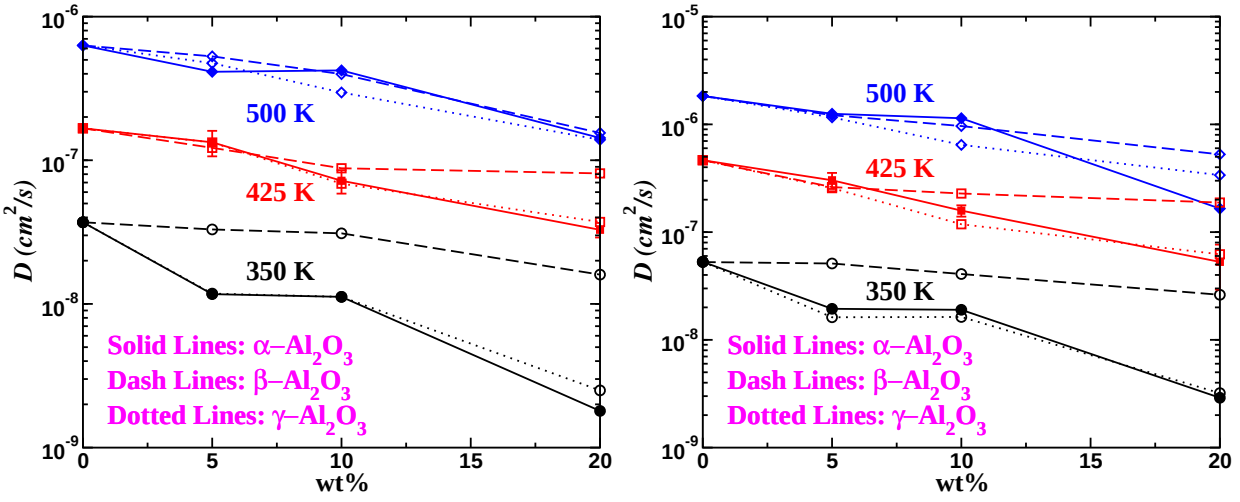

(a) Li^+ (b) BF_4^-

Figure 1: Diffusion coefficient of (a) Li^+ cations and (b) BF_4^- anions at EO:Li=15:1 as a function of the nanoparticle's loading in the presence of α, β and γ-Al_2O_3 nanoparticles. Data for β-Al_2O_3 are reproduced from our earlier work.[14] Lines are guide to the eye.

More pertinent to the issues considered in the present work, with an increase in the loading of nanoparticles, we observe a monotonic decrease in D for both types of ionic species at all the temperatures and for all types of nanoparticles. In comparing the influence of surface

chemistry of nanoparticles, we observe that with increasing particle loading there is a more significant reduction in D of the Li^+ and the BF_4^- ions for α and γ-Al_2O_3 nanoparticles when compared with the β-Al_2O_3 nanoparticles. Such a trend is most pronounced at 350 K and at higher particle loadings. However, the influence of surface chemistry is seen to become less important for higher temperatures and/or lower loadings of the nanoparticles.

3.1.2 Diffusivities at EO:Li=8:1

In Fig. 2, we display the ion diffusivity results for a salt concentration EO:Li=8:1. Overall, we observe that the qualitative trends seen at EO:Li=15:1 are preserved for EO:Li=8:1. In comparing Figs. 1 and 2, we observe that independent of the type of nanoparticle, the ion diffusivity values become lower when the salt concentration is increased from EO:Li=15:1 to EO:Li=8:1. In our previous work,[14] we suggested that such trends arose from the increased tendency of Li^+ ions to become coordinated with the polymer segments and the reduction in percolating paths for the motion of Li^+ ions due to the higher densities.

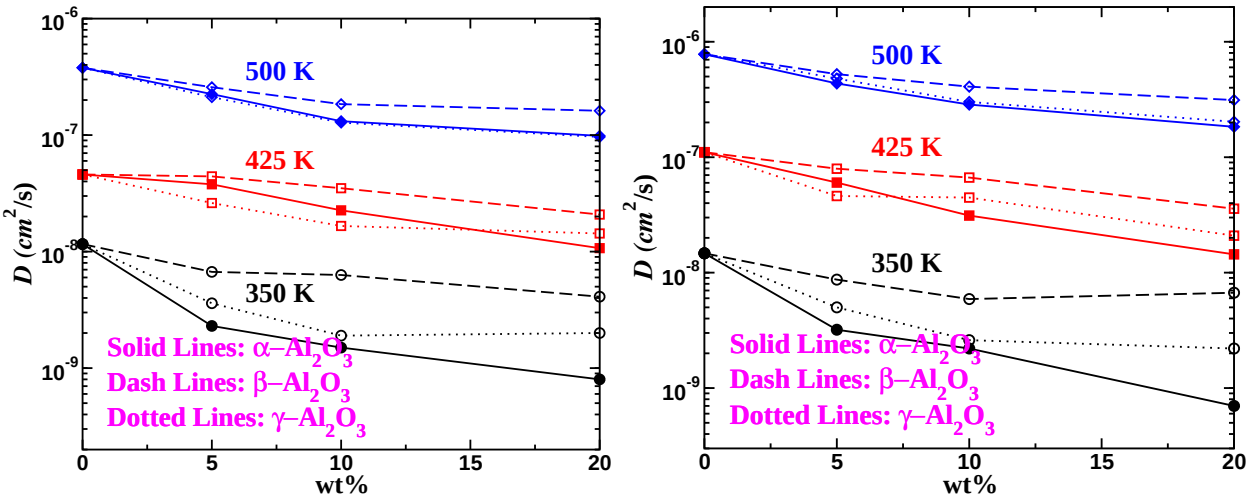

(a) Li^+ (b) BF_4^-

Figure 2: Diffusion coefficient of (a) Li^+ cations and (b) BF_4^- anions at EO:Li=8:1. Lines are a guide to the eye.

Interestingly, we observe that the surface chemistry of the nanoparticles has a stronger influence for the higher salt loading of EO:Li=8:1. Indeed, we observe that the diffusivities of

Li^+ ions in β-Al_2O_3 systems are higher than the results for α-Al_2O_3 and γ-Al_2O_3 systems even at high temperatures and low particle loadings, and such differences become even more pronounced with decreasing temperatures and increasing particle loadings. Moreover, γ-Al_2O_3 systems are seen to exhibit higher mobilities compared to α-Al_2O_3 systems. Similar trends are also seen to manifest in the context of BF_4^- ion diffusivities. These results indicate that the mobility of the ions in the PNC systems correlate inversely with the acidity of the nanoparticles, and that the influence of the latter becomes more pronounced with an increase in salt concentration.

3.2 Ionic Conductivity of PEO-$LiBF_4$ Electrolyte

Since ionic conductivity is a key property of interest in polymer electrolytes, in this section, we present results for the influence of the presence of various types of nanoparticles upon the ionic conductivities. In general, the behaviors of the ionic conductivities and the diffusion coefficients of the ions are expected to closely mirror each other at conditions corresponding to dilute concentration of the ions. However, with increase in the salt concentration, ion correlation effects become important and the ionic conductivities may exhibit trends which differ from the ionic mobilities.

Figure 3 displays ionic conductivities as a function of the loading of α, β and γ-Al_2O_3 nanoparticles for: (a) EO:Li=15:1; and (b) EO:Li=8:1 salt concentrations (the conductivities for the β-Al_2O_3 nanoparticle system were obtained from Ref. 14). The conductivities are seen to increase with the temperature, a result consistent with the observations for D of ionic species. Similar to the results observed for the D of ions, σ decreases monotonically for all α, β and γ-Al_2O_3 nanoparticle systems when the nanoparticle loading is increased.

In comparing the influence of the nanoparticle surface chemistry, we observe trends which are qualitatively consistent with the results noted in the context of the diffusivity of the ions. Explicitly, it can be seen that the conductivities for α-Al_2O_3 and γ-Al_2O_3 are typically lower than the values for β-Al_2O_3 systems. Moreover, it is evident that increasing particle loadings and salt concentrations accentuate the differences between the β-Al_2O_3 and the α-Al_2O_3, γ-Al_2O_3 sys-

tems. Moreover, we observe that the conductivities of α-Al_2O_3 are slightly greater than γ-Al_2O_3 systems for EO:Li=15:1, but, for the higher salt concentration of EO:Li=8:1, γ-Al_2O_3 systems possess larger conductivities than α-Al_2O_3 systems.

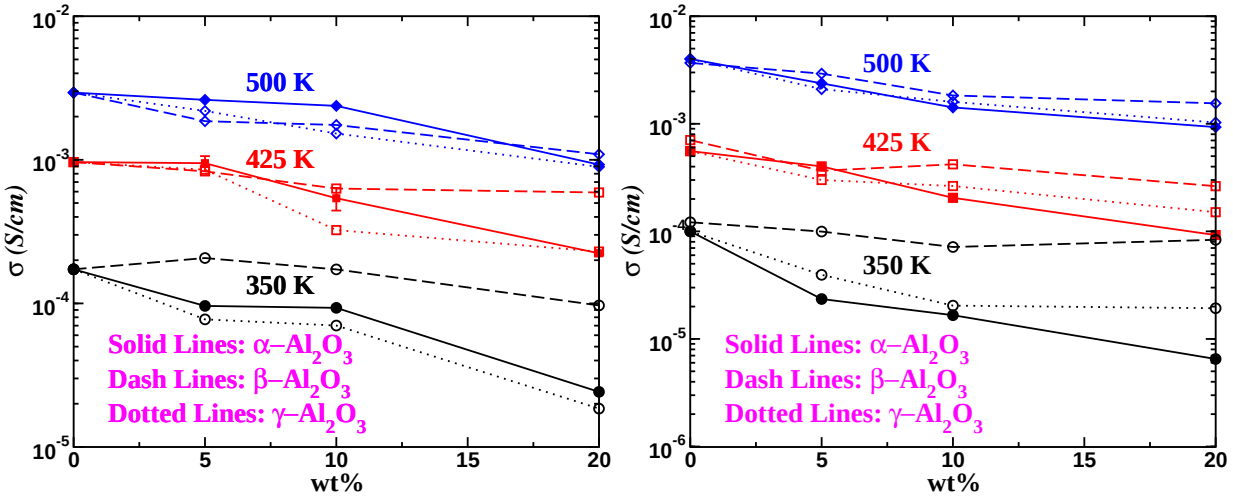

(a) EO:Li=15:1 (b) EO:Li=8:1

Figure 3: Ionic conductivity of PEO-$LiBF_4$ electrolyte as a function of the nanoparticles loading at all the temperatures at (a) EO:Li=15:1 and (b) EO:Li=8:1. Lines are a guide to the eye.

We note that the results presented in Fig. 3 are partially in agreement with recent experimental results of Ganapatibhotla and Maranas.[22] Explicitly, they found that conductivities of PNC systems containing α-Al_2O_3 nanoparticles were generally higher than that of the γ-Al_2O_3 nanoparticle systems. Such observations agree with our results for low salt loadings corresponding to EO:Li=15:1. However, for higher salt loadings corresponding to EO:Li=8:1, our results suggest that the α-Al_2O_3 nanoparticle systems possess the lowest conductivity. Moreover, Ref. 22 also reports regimes where the conductivity of α-Al_2O_3 nanoparticle system are higher than that of the pristine polymer matrix. However, such conditions are not evident in our results. While we do not have a conclusive explanation for the differences between the experiments and our results, we note that our simulations only probe the amorphous phases of the polymer electrolyte. Polymer crystallinity effects which have been speculated to be important in determining the conductivity of polymer electrolytes are absent in our framework and may contribute to such discrepancies.[6] In addition, we recall that in our work we represented α-Al_2O_3 and

γ-Al_2O_3 through simple modifications to the force fields. A more rigorous parametrization may potentially lead to different trends.

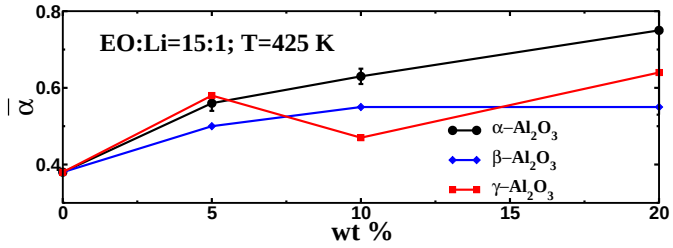

Figure 4: The average values of the degree of uncorrelated ion motion ($\bar{\alpha}$) in presence of the α, β and γ-Al_2O_3 nanoparticles. Lines are a guide to the eye.

Since σ reflects the influence of both ion diffusivities and ion correlation effects, it is of interest to consider the average degree of uncorrelated ion motion, $\bar{\alpha}$ (cf. section 2.4) to examine the influence, if any, of the surface chemistry of the nanoparticles. In Fig. 4 we display $\bar{\alpha}$ in presence of the α, β and γ-Al_2O_3 nanoparticles at EO:Li=15:1 and 425 K. We show the results for other temperatures and other salt loadings in Fig. S5 of ESI. In all our results, we observe that $\bar{\alpha}$ increases as a function of nanoparticle loading. Moreover, we find that $\bar{\alpha}$ increases with the degree of acidity of the nanoparticle, indicating a reduction in the ion correlations with the addition of nanoparticles.

4 Mechanisms Underlying Ion Mobilities and Conductivities

The previous section presented the results for the ionic mobilities and conductivities of nanoparticle dispersed systems. In all cases, we observed that ionic mobilities decreased with increased particle loading. With increasing acidity of the nanoparticles, i. e. transitioning from β-Al_2O_3 to γ-Al_2O_3, α-Al_2O_3 nanoparticles, three main results were noted: (i) The mobility of the ions decreased for both EO:Li=15:1 and EO:Li=8:1 salt concentrations, with the effects being more pronounced for EO:Li=8:1 systems; (ii) $\bar{\alpha}$ increases, suggesting a reduction in the ion correlations; and (iii) Conductivity, which is a product of ion mobilities and $\bar{\alpha}$ was also reduced. However, due to the opposite trends of the mobilities and $\bar{\alpha}$, the relative conductivities of α-Al_2O_3 and

γ-Al_2O_3 nanoparticles were dependent on the salt loading.

In the following sections, we focus on unraveling the mechanisms underlying the changes in ionic mobilities and conductivities and the influence of the acidity of the nanoparticles.

4.1 Polymer Segmental Dynamics

In our previous article[14] we demonstrated that as a consequence of the interactions between polymer, ions and the nanoparticles, the polymer dynamics in PNC systems can be quite different when compared to nanoparticle-free systems. Motivated by such results, we investigated the polymer dynamics in the *ion-doped* polymer nanocomposites for the systems studied in this work.

In Fig. 5, we present results for the mean polymer segmental relaxation time calculated using Eq 9 for all the systems at EO:Li=15:1(results for EO:Li=8:1 are shown in Fig. S6 of ESI). We observe that τ decreases monotonically with increasing temperature, an observation which correlates with the temperature dependence of the D of ions. In considering the effect of nanoparticles, we observe that irrespective of the underlying surface chemistry, τ increases with loading of the nanoparticles. More pertinently, we observe that τ increases with increasing acidity of the nanoparticles. The latter observation is consistent with results reported by Ganapatibhotla and Maranas[22] for *ion-free* nanocomposites.

In our previous study,[14] we demonstrated that the changes in polymer segmental mobilities in PNC systems were a manifestation of the influence of the nanoparticles on the dynamics of polymer segments in their vicinity. Explicitly, by probing an "interfacial zone" around the nanoparticles, we showed that the polymer segmental dynamics in such a region was significantly hindered relative to the bulk regions of the electrolyte. Moreover, our results suggested that such effects arose from the interactions between the polymer and the nanoparticle, and hence were present even for *ion-free* systems. However, the presence of ions led to a further slowing (by approximately the same relative amount) of the polymer dynamics[43–45] in the bulk and the interfacial zones.

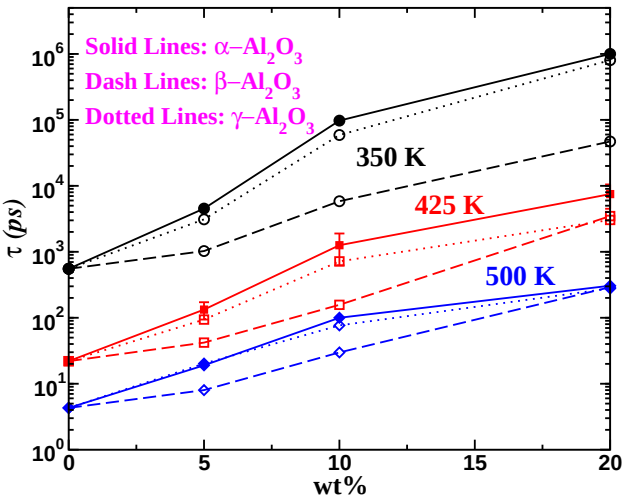

Figure 5: Mean of the segmental relaxation times of the PEO chains as a function of the Al_2O_3 weight percentage at different temperatures and EO:Li=15:1. Lines are a guide to the eye.

Inspired by the above findings, we probed the spatially resolved polymer dynamics in both *ion-free* and *ion-doped* systems for different surface chemistries of the nanoparticles. Fig. 6 displays the mean relaxation times of polymer chains in the "near" and "far" zones for α-Al_2O_3 and γ-Al_2O_3 nanoparticle systems. Overall, with the introduction of nanoparticles, we observe that the polymer dynamics is slowed in the "near" region compared to the "far" region. When we compare the mean segmental relaxation times of the *ion-doped* systems with the *ion-free* systems, we observe that the relaxations in the *ion-doped* systems are slower than those in the *ion-free* system (however, the relative values of the near and far time scales for *ion-free* and *ion-doped* systems, which are not displayed, were found to be approximately the same).

In relation to the surface chemistry of the nanoparticles, we observe in Fig. 6 that the relaxation times in the interfacial zone increases with increasing acidity of the nanoparticles. A number of other studies have suggested that the extent of slowing of the polymer dynamics near surfaces to be directly correlated to the strength of polymer-surface interfacial interactions.[46,47] In the present situation, we note that H atoms on the surface of the nanoparticles exhibits an affinity to EO of the polymer backbone. Since the number of H atoms on nanoparticle's surface increases with the degree of acidity, the strength of the attraction be-

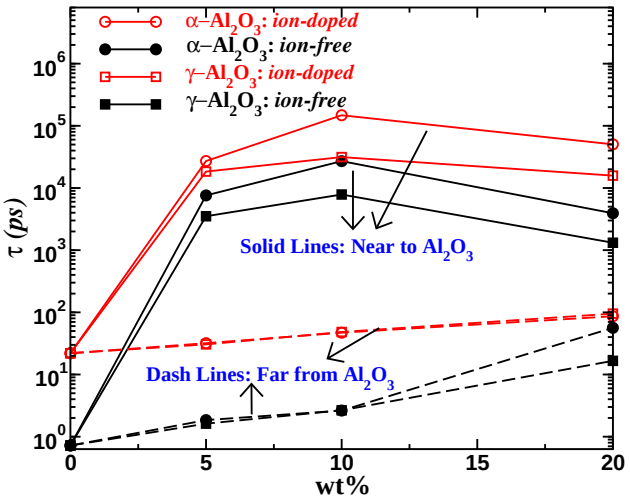

Figure 6: Polymer segmental relaxations in the interfacial zone for the *ion-doped* and *ion-free* systems in the presence of α-Al_2O_3 and γ-Al_2O_3 nanoparticles for EO:Li=15:1 and 425 K.

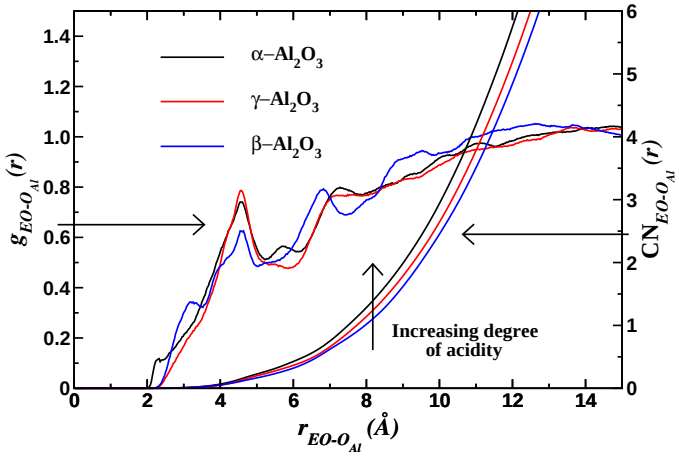

Figure 7: Partial radial distribution of the polymer-nanoparticle structure and corresponding coordination number at 425 K with the loading of α, β and γ-Al_2O_3 nanoparticles at 5 wt%.

tween nanoparticles and polymer is also likely to increase with the degree of acidity. To corroborate such a hypothesis, in Fig. 7 we display a comparison of the partial radial distribution functions of polymer-nanoparticle (EO-O_{Al}) structure and corresponding coordination numbers for α, β and γ-Al_2O_3 nanoparticles. Consistent with our hypothesis, when we compare the more acidic α-Al_2O_3 and γ-Al_2O_3 systems with β-Al_2O_3 nanoparticles, we observe increased polymer-particle correlations in the former as reflected in $g(r)$ and the coordination numbers.

Together, the results of Figs. 6 and 7 serve to rationalize both the influence of particle loadings and the role of particle acidity upon the relaxation times of the polymer matrix (cf. Fig. 5).

Indeed, with increase in the loading of nanoparticles, the volume occupied by the interfacial regions are expected to increase relative to the volume occupied by the bulk of the polymer. Hence, the system-averaged polymer relaxation times are expected to increase with the loading of the nanoparticles (Fig. 6). Moreover, since increasing acidity is seen to exert stronger influence upon the polymer relaxation behavior, the overall relaxation times are slower for α-Al_2O_3, γ-Al_2O_3 nanoparticles relative to β-Al_2O_3 systems.

4.2 Correlation Between Polymer Dynamics and Diffusion of Ions

A number of experimental and simulation studies have demonstrated that the segmental mobility of polymer chains in the polymer electrolytes has a direct influence upon the ion transport properties.[19,20,28,30,31,48,49] In our previous study of PNCs containing β-Al_2O_3 nanoparticles,[14] we demonstrated that the influence of nanoparticles on the ion diffusivities can be *quantitatively* correlated to the polymer segmental dynamics in the presence of ions and nanoparticles. Such a result was somewhat surprising since it suggested that the influence of the nanoparticle arose exclusively through its impact upon the polymer dynamics, and that other changes in equilibrium and dynamical characteristics arising from the introduction of nanoparticles had at-best only a small quantitative effect.

Motivated by the findings in our previous work, in Fig. 8, we directly compare the Li^+ ion mobilities and the polymer segmental mobilities, τ^{-1} (the β-Al_2O_3 results from our previous work are displayed in Fig. S7 of ESI). In the particle-free polymer melt, we observe a good correlation between the changes in the polymer segmental mobilities with temperature and the corresponding effects on anionic and cationic mobilities. With increase in particle loading, the correlations between the segmental dynamics and the ion mobilities are seen to broadly persist for both α-Al_2O_3 and γ-Al_2O_3 nanoparticles. However, for higher nanoparticle loadings, the correlations between D_{Li} and τ^{-1} are seen to exhibit visible quantitative deviations. Moreover, the deviations are seen to be more pronounced for α-Al_2O_3 nanoparticles when compared with γ-Al_2O_3 nanoparticles, suggesting that increasing particle acidity contributes to such effects.

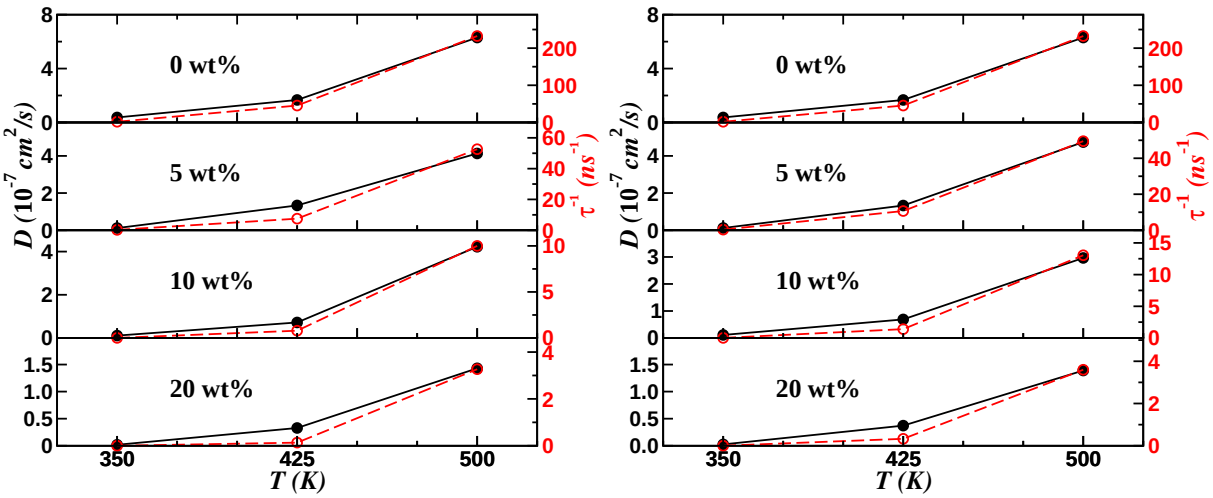

(a) α-Al_2O_3 (b) γ-Al_2O_3

Figure 8: Correlation between diffusion of ions and polymer segmental dynamics: D of Li^+ ions shown as filled symbols with bold lines and τ^{-1} shown as open symbols with dash lines as a function of the temperature at various loading of the nanoparticles at EO:Li=15:1 in the presence of (a) α-Al_2O_3 nanoparticles and (b) γ-Al_2O_3 nanoparticles. Lines are a guide to the eye.

Interestingly, we observe that in almost all cases the diffusivities are faster than what may be expected based on the polymer segmental relaxation times.

The above results confirm that the nanoparticle-induced changes in the polymer segmental dynamics does play the dominant role in the observed changes in the ionic mobilities, and that such a mechanism persists even with modifications to the surface chemistry of the nanoparticles. However, the deviations noted in the comparison of the correlations between the polymer segmental relaxation time and the ion diffusivity suggests that with increasing acidity of the nanoparticles other mechanisms may also possibly influence the ionic mobilities. In the next section, we present results for the coordination characteristics of the ions to help explain such findings.

4.3 Effects of Particle Acidity on Ion Coordination

To reveal the other mechanisms of influence of the nanoparticles on ion mobilities, we probed the coordination number (CN) of various atoms and display them in Fig. 9. The arrows in the Fig. 9 indicate changes with increasing degree of acidity on the nanoparticles. From the results

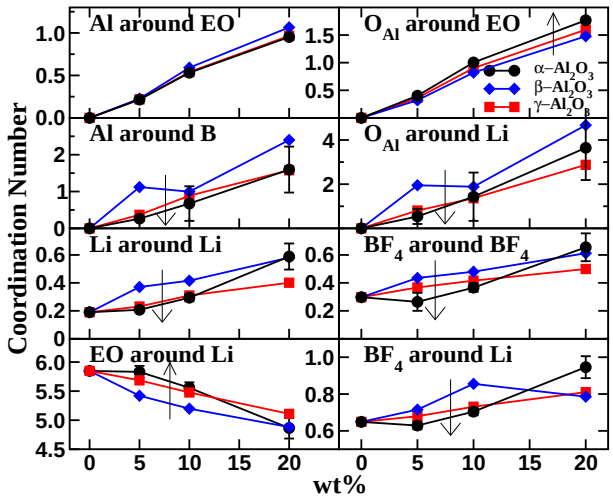

Figure 9: Factors affecting conductivity of polymer nanocomposites in the presence of α, β and γ-Al_2O_3 nanoparticles: coordination numbers (CN) of various atoms in the specified atomic local environment.

for the coordination between O_{Al} and EO units, we deduce that increasing the acidity of the nanoparticle enhances the coordination of the polymer segments with the nanoparticle. Such results mirror the trends and implications discussed in Section 4.1. More interestingly, the coordination number results Al-B and O_{Al}-Li suggests that an enhancement in the acidity of the nanoparticle leads to a decrease in the coordination between the nanoparticle and the ions. While these trends may be expected in the case of Li^+ ions due to the repulsive interactions between acidic sites and Li^+ ions, more surprisingly, we also observe repulsion of BF_4^- ions from acidic surfaces despite the ability of BF_4^- ions to form H-bonds with acidic sites. We speculate that the enhanced interactions between the polymer and the acidic nanoparticles may be a contributing factor for such a result.

The above results provide insights into the quantitative deviations observed in Section 4.2 between the diffusivities and the segmental relaxation times. In general, we expect that a strict correlation between the polymer segmental dynamics and the ion mobilities to apply if the ion coordination with the nanoparticle follows the same trends as the polymer coordination characteristics. The above results however indicate that with increasing acidity, there are differences in the distribution of ions relative to the nanoparticle centers. Explicitly, for α-Al_2O_3 and

γ-Al_2O_3 systems more (relative to β-Al_2O_3 nanoparticles) Li^+ and BF_4^- ions are likely to be found away from the interfacial zone near the particles. This would suggest that the ion mobilities "sample" a larger fraction of polymer regions possessing higher mobilities. Such an explanation also rationalizes our observation in Section 4.2 that the diffusivities were in general larger than what may be expected based on polymer segmental mobilities. In sum, we suggest that because of the increased acidity of the nanoparticles, less Li^+ ions exist in the interfacial zone and are hence less influenced by the changes in polymer dynamics therein. As a consequence, the mobility of Li^+ ions do not strictly follow the averaged segmental dynamics of the polymer.

A second interesting result in Fig. 9 is that increasing acidity of the nanoparticle is seen to weaken both the Li-Li and BF_4-BF_4 coordinations. Speculatively, such effects may be a consequence of the enhanced repulsions of the Li^+ ions from the particle surface, which may result in an enhanced coordination between EO and Li^+ ions at the expense of other interactions. The weakened coordination between the anions and cations serve to explain the increase with acidity of the extent of uncorrelated ion motion seen in Fig. 4.

5 Summary

We investigated the influence of surface chemistry of nanoparticles on ion transport mechanisms in polymer electrolytes. We modeled α-Al_2O_3 and γ-Al_2O_3 nanoparticles by using an appropriate distribution of acidic sites on the surface. Ion diffusivities, ionic conductivities and polymer dynamics were studied as a function of the loading of the nanoparticles. With increasing loading of the nanoparticles, we observed reduced ionic mobilities and conductivities compared to *pure* PEO melt. The observed diffusivities of ionic species correlated well with the polymer segmental dynamics with however quantitative deviations apparent for higher particle loadings. The influence of nanoparticles on the polymer dynamics was rationalized through the preferential interactions between the polymer segments and the surface. Quantitative disparities between ionic mobilities and polymer segmental dynamics were justified by invoking

the changes in local environment of ions in the electrolyte.

Specific to the influence of surface chemistry, we observed that the polymer-particle interactions were stronger for more acidic nanoparticles, and hence interfacial effects lead to a stronger reduction in the mobilities of the polymer segments and the ions. In addition, the changes in local ion environment correlated with the acidity of the nanoparticles. In sum, the combined effects of the influence of nanoparticles on the polymer segmental dynamics and the changes in local environment of ions were found to be the key factors controlling ion transport in polymer nanocomposites.

The results of the present work when viewed in conjunction with those reported in our previous article[14] helps identify universal aspects in the mechanisms of influence of nanoparticles on ion mobilities in PNCs. Indeed, the polymer-nanoparticle interactions are seen to be a key in influencing the changes in local polymer segmental dynamics. Nanoparticle-ion interactions are also seen to play an important role in modulating the distribution of ions in the system and thereby tracks the correlations between the modified polymer segmental dynamics and the macroscopic ion mobilities. In addition, nanoparticle-ion interactions are also seen to indirectly influence the ion-ion coordination behavior and thereby the macroscopic conductivities. Such findings suggest that by appropriately tuning the nanoparticle-polymer and nanoparticle-ion interactions, it may be possibly achieve mobilities and conductivities higher than that of the pristine polymer matrix. In a future article, we plan to examine such a proposal and also identify the concomitant influence of such interactions upon the mechanical properties of the nanocomposite electrolyte.

6 Acknowledgement

We thank Prof. Collin D. Wick for clarifications regarding the force fields for acidic nanoparticles. The authors acknowledge the Texas Advanced Computing Center (TACC) at The University of Texas at Austin for providing computing resources that have contributed to the research

results reported within this paper. This work was supported in part by grants from Robert A. Welch Foundation (Grant F1599) and National Science Foundation (DMR-1306844) and the US Army Research Office under grant W911NF-13-1-0396.

References

(1) Armand, M. Polymer Solid Electrolytes - an Overview. *Solid State Ionics* **1983**, *9-10*, 745–754.

(2) Armand, M. B. Polymer Electrolytes. *Annu. Rev. Mater. Sci.* **1986**, *16*, 245–261.

(3) Springer, T. E.; Zawodzinski, T.; Gottesfeld, S. Polymer Electrolyte Fuel-cell Model. *J. Electrochem. Soc.* **1991**, *138*, 2334–2342.

(4) Meyer, W. H. Polymer electrolytes for lithium-ion batteries. *Adv. Mater.* **1998**, *10*, 439–448.

(5) Croce, F.; Appetecchi, G. B.; Persi, L.; Scrosati, B. Nanocomposite polymer electrolytes for lithium batteries. *Nature* **1998**, *394*, 456–458.

(6) Croce, F.; Curini, R.; Martinelli, A.; Persi, L.; Ronci, F.; Scrosati, B.; Caminiti, R. Physical and chemical properties of nanocomposite polymer electrolytes. *J. Phys. Chem. B* **1999**, *103*, 10632–10638.

(7) Tarascon, J. M.; Armand, M. Issues and challenges facing rechargeable lithium batteries. *Nature* **2001**, *414*, 359–367.

(8) Christie, A. M.; Lilley, S. J.; Staunton, E.; Andreev, Y. G.; Bruce, P. G. Increasing the conductivity of crystalline polymer electrolytes. *Nature* **2005**, *433*, 50–53.

(9) Arico, A. S.; Bruce, P. G.; Scrosati, B.; Tarascon, J. M.; Van Schalkwijk, W. Nanostructured materials for advanced energy conversion and storage devices. *Nat. Mater.* **2005**, *4*, 366–377.

(10) Bruce, P. G.; Scrosati, B.; Tarascon, J.-M. Nanomaterials for rechargeable lithium batteries. *Angew. Chem.-Int. Edit.* **2008**, *47*, 2930–2946.

(11) Smitha, B.; Sridhar, S.; Khan, A. A. Solid polymer electrolyte membranes for fuel cell applications - a review. *J. Membr. Sci.* **2005**, *259*, 10–26.

(12) Hallinan, D. T., Jr.; Balsara, N. P. Polymer Electrolytes. *Annu. Rev. Mater. Res.* **2013**, *43*, 503–525.

(13) Fullerton-Shirey, S. K.; Maranas, J. K. Structure and Mobility of PEO/$LiClO_4$ Solid Polymer Electrolytes Filled with Al_2O_3 Nanoparticles. *J. Phys. Chem. C* **2010**, *114*, 9196–9206.

(14) Mogurampelly, S.; Ganesan, V. Effect of Nanoparticles on Ion Transport in Polymer Electrolytes. *Macromolecules* **2015**, *48*, 2773–2786.

(15) Kasemägi, H.; Klintenberg, M.; Aabloo, A.; Thomas, J. O. Molecular dynamics simulation of the effect of adding an Al_2O_3 nanoparticle to PEO-LiCl/LiBr/LiI systems. *J. Mater. Chem.* **2001**, *11*, 3191–3196.

(16) Kasemägi, H.; Klintenberg, M.; Aabloo, A.; Thomas, J. O. Molecular dynamics simulation of the $LiBF_4$-PEO system containing Al_2O_3 nanoparticles. *Solid State Ionics* **2002**, *147*, 367–375.

(17) Borodin, O.; Smith, G. D.; Bandyopadhyaya, R.; Redfern, P.; Curtiss, L. A. Molecular dynamics study of nanocomposite polymer electrolyte based on poly(ethylene oxide)/$LiBF_4$. *Model. Simul. Mater. Sci. Eng.* **2004**, *12*, S73–S89.

(18) Borodin, O.; Smith, G. D.; Bandyopadhyaya, R.; Byutner, E. Molecular dynamics study of

the influence of solid interfaces on poly(ethylene oxide) structure and dynamics. *Macromolecules* **2003**, *36*, 7873–7883.

(19) Hanson, B.; Pryamitsyn, V.; Ganesan, V. Mechanisms Underlying Ionic Mobilities in Nanocomposite Polymer Electrolytes. *ACS Macro Lett.* **2013**, *2*, 1001–1005.

(20) Berthier, C.; Gorecki, W.; Minier, M.; Armand, M. B.; Chabagno, J. M.; Rigaud, P. Microscopic investigation of ionic conductivity in alkali metal salts-poly(ethylene oxide) adducts. *Solid State Ionics* **1983**, *11*, 91–95.

(21) Lin, K.-J.; Li, K.; Maranas, J. K. Differences between polymer/salt and single ion conductor solid polymer electrolytes. *RSC Adv.* **2013**, *3*, 1564–1571.

(22) Ganapatibhotla, L. V. N. R.; Maranas, J. K. Interplay of Surface Chemistry and Ion Content in Nanoparticle-Filled Solid Polymer Electrolytes. *Macromolecules* **2014**, *47*, 3625–3634.

(23) Ganesan, V.; Jayaraman, A. Theory and simulation studies of effective interactions, phase behavior and morphology in polymer nanocomposites. *Soft Matter* **2014**, *10*, 13–38.

(24) Wieczorek, W.; Zalewska, A.; Raducha, D.; Florjanczyk, Z.; Stevens, J. R. Composite polyether electrolytes with Lewis acid type additives. *J. Phys. Chem. B* **1998**, *102*, 352–360.

(25) Wu, H.; Cummings, O. T.; Wick, C. D. Computational Investigation on the Effect of Alumina Hydration on Lithium Ion Mobility in Poly(ethylene oxide) $LiClO_4$ Electrolytes. *J. Phys. Chem. B* **2012**, *116*, 14922–14932.

(26) Eilmes, A.; Kubisiak, P. Molecular Dynamics Study on the Effect of Lewis Acid Centers in Poly(ethylene oxide)/$LiClO_4$ Polymer Electrolyte. *J. Phys. Chem. B* **2011**, *115*, 14938–14946.

(27) Smith, G. D.; Yoon, D. Y.; Jaffe, R. L.; Colby, R. H.; Krishnamoorti, R.; Fetters, L. J. Conformations and structures of poly(oxyethylene) melts from molecular dynamics

simulations and small-angle neutron scattering experiments. *Macromolecules* **1996**, *29*, 3462–3469.

(28) Müller-Plathe, F. Permeation of polymers - A computational approach. *Acta Polym.* **1994**, *45*, 259–293.

(29) Neyertz, S.; Brown, D. Local structure and mobility of ions in polymer electrolytes: A molecular dynamics simulation study of the amorphous PEO(x)NaI system. *J. Chem. Phys.* **1996**, *104*, 3797–3809.

(30) Borodin, O.; Smith, G. D. Mechanism of ion transport in amorphous poly(ethylene oxide)/LiTFSI from molecular dynamics simulations. *Macromolecules* **2006**, *39*, 1620–1629.

(31) Borodin, O.; Smith, G. D.; Douglas, R. Force field development and MD simulations of poly(ethylene oxide)/$LiBF_4$ polymer electrolytes. *J. Phys. Chem. B* **2003**, *107*, 6824–6837.

(32) Borodin, O.; Smith, G. D. Development of quantum chemistry-based force fields for poly(ethylene oxide) with many-body polarization interactions. *J. Phys. Chem. B* **2003**, *107*, 6801–6812.

(33) Edvardsson, S.; Klintenberg, M.; Thomas, J. Use of polarized optical absorption to obtain structural information for Na^+/Nd^{3+} β"-alumina. *Phys. Rev. B* **1996**, *54*, 17476–17485.

(34) Gutierrez, G.; Belonoshko, A.; Ahuja, R.; Johansson, B. Structural properties of liquid Al2O3: A molecular dynamics study. *Phys. Rev. E* **2000**, *61*, 2723–2729.

(35) Plimpton, S. Fast Parallel Algorithms for Short-Range Molecular Dynamics. *J. Comput. Phys.* **1995**, *117*, 1–19.

(36) Borodin, O.; Gorecki, W.; Smith, G. D.; Armand, M. Molecular Dynamics Simulation and Pulsed-Field Gradient NMR Studies of Bis(fluorosulfonyl)imide (FSI) and

Bis[(trifluoromethyl)sulfonyl]imide (TFSI)-Based Ionic Liquids. *J. Phys. Chem. B* **2010**, *114*, 6786–6798.

(37) Li, Z.; Smith, G. D.; Bedrov, D. Li+ Salvation and Transport Properties in Ionic Liquid/Lithium Salt Mixtures: A Molecular Dynamics Simulation Study. *J. Phys. Chem. B* **2012**, *116*, 12801–12809.

(38) Lesch, V.; Jeremias, S.; Moretti, A.; Passerini, S.; Heuer, A.; Borodin, O. A Combined Theoretical and Experimental Study of the Influence of Different Anion Ratios on Lithium Ion Dynamics in Ionic Liquids. *J. Phys. Chem. B* **2014**, *118*, 7367–7375.

(39) Picalek, J.; Kolafa, J. Molecular dynamics study of conductivity of ionic liquids: The Kohlrausch law. *J. Mol. Liq.* **2007**, *134*, 29–33.

(40) Ndoro, T. V. M.; Boehm, M. C.; Müller-Plathe, F. Interface and Interphase Dynamics of Polystyrene Chains near Grafted and Ungrafted Silica Nanoparticles. *Macromolecules* **2012**, *45*, 171–179.

(41) Smith, G. D.; Borodin, O.; Bedrov, D.; Paul, W.; Qiu, X. H.; Ediger, M. D. C-13 NMR spin-lattice relaxation and conformational dynamics in a 1,4-polybutadiene melt. *Macromolecules* **2001**, *34*, 5192–5199.

(42) Smith, G. D.; Borodin, O.; Paul, W. A molecular-dynamics simulation study of dielectric relaxation in a 1,4-polybutadiene melt. *J. Chem. Phys.* **2002**, *117*, 10350–10359.

(43) Vogel, M.; Torbruegge, T. Ion and polymer dynamics in polymer electrolytes PPO-LiClO4. I. Insights from NMR line-shape analysis. *J. Chem. Phys.* **2006**, *125*, 054905.

(44) Vogel, M.; Torbruegge, T. Ion and polymer dynamics in polymer electrolytes PPO-LiClO4 .II. H-2 and Li-7 NMR stimulated-echo experiments. *J. Chem. Phys.* **2006**, *125*, 164910.

(45) Fullerton-Shirey, S. K.; Maranas, J. K. Effect of LiClO4 on the Structure and Mobility of PEO-Based Solid Polymer Electrolytes. *Macromolecules* **2009**, *42*, 2142–2156.

(46) Starr, F. W.; Schroder, T. B.; Glotzer, S. C. Effects of a nanoscopic filler on the structure and dynamics of a simulated polymer melt and the relationship to ultrathin films. *Phys. Rev. E* **2001**, *64*, 021802.

(47) Kropka, J. M.; Pryamitsyn, V.; Ganesan, V. Relation between glass transition temperatures in polymer nanocomposites and polymer thin films. *Phys. Rev. Lett.* **2008**, *101*, 075702.

(48) Gadjourova, Z.; Andreev, Y. G.; Tunstall, D. P.; Bruce, P. G. Ionic conductivity in crystalline polymer electrolytes. *Nature* **2001**, *412*, 520–523.

(49) Diddens, D.; Heuer, A. Simulation Study of the Lithium Ion Transport Mechanism in Ternary Polymer Electrolytes: The Critical Role of the Segmental Mobility. *J. Phys. Chem. B* **2014**, *118*, 1113–1125.